Available online at www.sciencedirect.com
SCIENCE DIRECT
Catalysis Today 101 (2005) 53–64
CATALYSIS TODAY
www.elsevier.com/locate/cattod

Bimetallic nano-particles: featuring structure and reactivity

László Guczi [a,b,*]

[a] Department of Surface Chemistry and Catalysis, Institute of Isotopes, CRC, HAS, P.O. Box 77, H-1525 Budapest, Hungary
[b] Laboratory for Nanostructured Metal Catalysts, Institute of Surface Chemistry and Catalysis, CRC, HAS Pusztaszeri u. 59/67, 1121 Budapest, Hungary

Abstract

Highly dispersed, oxide- or zeolite-supported bimetallic catalysts are widely used in the catalytic industry, such as in catalytic reforming, nitrogen industry and gas-to-liquid technology. The paper highlights the nano-sized bimetallic system in terms of correlation between structure and reactivity/selectivity promoted by the second metal. Opposite to the bulk alloys nano-sized bimetallic catalysts are extremely sensitive to the structure, morphology, valence state of the supporting oxide material in which the nano-particles are embedded. In this case, one of the less reducible components, which strongly interact with the supports, may stabilize the second, more noble metals, and thus the latter can be stabilized in highly dispersed state. Conversely, addition of noble metal to the hardly reducible component may facilitate reduction, which causes the retardation of the deactivation process of some hydrocarbon reaction.

The future trend is the application of bimetallic nano-particles although careful consideration and experimentation should be taken to elucidate the structure of such type of catalyst.

The various effects of bimetallic particles, such as particle size, metal/support interface, morphology and electronic effects, on the activity/selectivity in given catalytic reactions will be discussed.

Keywords: Bimetallic nano-structured catalysts; Activity/selectivity relationship

1. Introduction

1.1. Historical background

Because of the importance of alloys in catalysis, much effort has been devoted to understand the origin of the catalytic effects. The rigid band model (RBM) developed by Dowden and Reynolds [1] was found to explain reactivity of NiCu alloys for benzene hydrogenation, however, it failed when ethylene was hydrogenated over NiCu alloys where no loss in activity was observed at 60 at.% copper [2]. The most comprehensive studies describing various limiting factors for behavior of alloys in connection with catalysis were put forward in 1970s [3–13] and in 1990s [14,15]. The starting point in explaining the effect of bimetallic catalysts was that metals generally maintain their individuality (e.g. valence band structures) in alloy [4].

The alloy formation in bulk system is always a function of thermodynamics. The magnitude and sign of entropy changes (ΔS) dictates the structure of bimetallic species:

- when ΔS is near to zero: almost ideal solutions are formed;
- when ΔS is small and negative: the result is a solid or a regular solution provided that the difference in atomic radii is no more negligible (e.g. Pt–Cu);
- when ΔS is large and negative: intermetallic compounds or ordered solutions are formed. From catalytic points of view some interesting intermetallic compounds are similar to chemical compounds;
- when ΔS is small and positive: mono- or bi-phasic alloy exist depending on the temperature of equilibration (e.g. Ni–Cu);
- when ΔS is large and positive: surface alloying or often clusters formation (Ru–Cu) occurs.

However, on alloying, the local density of states (LDOS) are subjected to a change and the d-bands are narrowed. Since chemical bonds are formed by overlapping the metal

* Tel.: +36 1 392 2534; fax: +36 1 392 2703.
E-mail address: guczi@sunserv.kfki.hu.

0920-5861/$ – see front matter © 2005 Elsevier B.V. All rights reserved.
doi:10.1016/j.cattod.2005.01.002

d-band with the molecular orbital of the substrates, any changes in the LDOS affects the chemisorption bonds.

1.2. Early theory for bimetallic systems

One of the early phenomena investigated in bimetallic catalysis was the segregation of metal on the surface as catalysis is controlled by the surface composition, which deviates from that of bulk. Generally,

(1) In solid solutions, surface enrichment in the component with lower heat of sublimation increases with decreasing coordination of the surface atoms [5]. This enrichment is less pronounced at higher temperature. It depends on whether alloy formation is endothermic or exothermic. For endothermic alloy formation ($\Delta S < 0$), enrichment in the component with the lower heat of sublimation occurs. The degree of enrichment is highest at higher index faces, edges, and corners. If the alloy formation were exothermic ($\Delta S > 0$), depletion in the second layer by a component that becomes enriched in the surface layer would occur.
(2) Biphasic alloys exist if there is a miscibility gap in the phase diagram of the alloy. At equilibrium each crystallite consists of a kernel enveloped in a skin of different alloys.

The so-called 'cherry model' [6] consists of three concentric spheres, which depend on the relative surface tensions.

According to the broken bond approximation [16,17], in perfect solutions the component with lower heat of vaporization will be enriched at the surface and the degree of enrichment is highest at higher index faces, edges, and corners. Two basic phenomena control segregation: (i) size differences, which lead to lattice strain energy; (ii) difference in the heat of vaporization of the components. Enrichment is therefore crystal-face dependent and decreases with increasing temperature. Several side effects influence surface segregation. One of the most important is the effect of the component size. Oversized atoms implanted in an ideal crystal lattice cause compression, which results in higher strain energy than occurs with undersized atoms. Thus, oversized atoms tend to segregate to the surface. This is because at compression the energy curve increases steeply and creates a driving force that expels oversized atoms to a greater extent than occurs with undersized atoms.

On the other hand, it is well known that alloys are greatly affected by ambient gas atmosphere. Generally, the metal, which displays a higher reactivity towards the ambient gas, will be driven to the surface. For example, in oxygen the metal, which has a higher heat of oxidation will be segregated to the surface.

1.3. Theory of ensemble and ligand effects

One of the most critical areas where highly dispersed bi- or multi-metallic particles find utilization is heterogeneous catalysis. After RBM, the coherent potential approximation (CPA) became the determining theory in catalysis by alloys [14,16,17]. Based upon UPS and XPS measurements it was proved that for endothermic or weakly exothermic formed alloys the position of d-band does not change. The main effect on alloy formation is the narrowing d-bands, which results in a decrease of degree of overlapping the d-bands among the different components (see Fig. 1 [18]). The change in LDOS may influence electron transfer between the substrate and adsorbate molecules. As a result, in some cases (e.g. CO–metal system) the bond strength between CO molecules and the metal has a strong affect on the ratio of dissociatively versus associatively adsorbed CO.

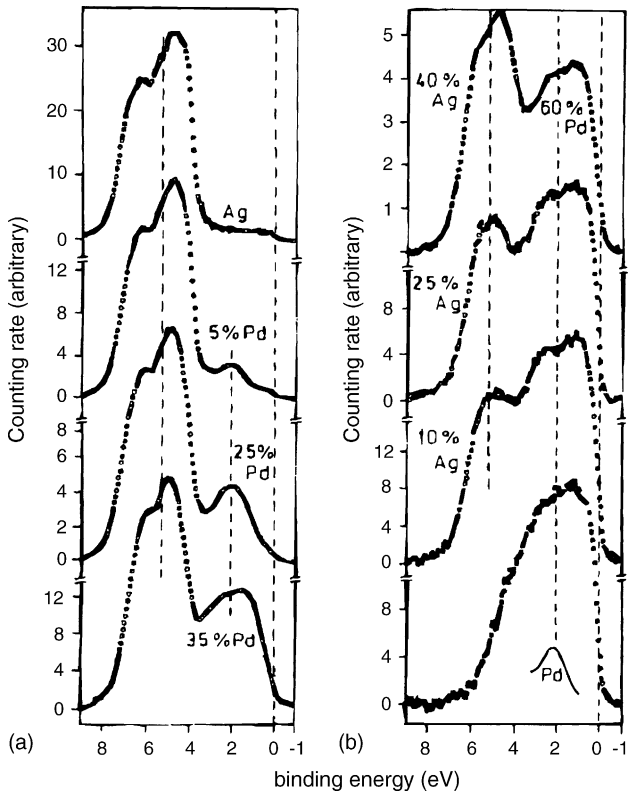

Fig. 1. Ultraviolet photoelectron spectra (UPS) of Pd–Ag alloy at various compositions [18].

Sachtler and van Santen [5,6], Sinfelt [19], Clarke [20], and Ponec and co-workers [4,21] introduced the ensemble and ligand effect. The idea was based mainly on selectivity data found previously for hydrocarbon reactions. It is well known that the modification of an active group VIII transition metal with IB metals greatly suppresses the catalytic activity for hydrocarbon reactions, which require a large number of neighboring surface atoms (ensembles). On the other hand, the reaction, which needs one metal adsorption site, is not affected. This means that primary ensemble size effect is defined by the dilution of the active ensemble with an 'inert' second metal [13,22].

While it is a relatively easy task to identify the ensemble size effect, the electronic or ligand effect is more elusive. The absence of important ligand effects has been attributed

to the experimental fact that alloying not, or only marginally, influences the chemisorption bond strength [13,23,25]. Moreover, it has been argued theoretically by van Santen [24] that metal–hydrogen and metal–carbon bond strengths are not altered by alloying of groups VIII with IB metals.

Normally, these factors govern the active-site arrangement at the surface for unsupported alloys in which case the particle size is large (in the range of several tens of nm). In practice, oxide- or zeolite-supported catalysts are employed, which requires some other phenomena to be taken into account.

1.4. Recent approaches to the structure of bimetallic catalysts

1.4.1. Electron transfer between components

The existence of electron transfer between metals has been clearly demonstrated in single crystal bimetallic samples. For example, the Co 2p line has a 0.5 eV binding energy (BE) shift towards higher values in PtCo single crystal [26,27]. A similar change in electron population was measured for PtZn alloying by work function measurements where a lower work function was measured for PtZn (4.33 eV) compared to that found for pure Pt (5.7 eV) [28]. In the same way, a 0.7 eV shift in BE was observed of Ag 3d core level BE when it was deposited over Pd (1 0 0) single crystal in PdAg [29].

Goodman and co-workers who measured electron transfer between alloys performed the most systematic study [30–35]. They evaporated a second metal in various amounts starting from submonolayer up to multilayer coverage onto a series of single crystal substrates and determined the core level BE. In this work, XPS studies were carried out on a variety of substrates (Ru, Rh, Ni, etc.) with copper being evaporated onto each from 0.25 to 10 ML (ML: monolayer). Below 1 ML there was no shift in the Cu $2p_{3/2}$ line indicating the formation of 2D islands. At higher coverage the Cu $2p_{3/2}$ BE increased monotonically. This increase was experienced on Cu/Rh (1 1 0), Cu/Ru (0 0 0 1) on Ni/Ru (0 0 0 1), whereas a decrease was measured on e.g. Pd/W (1 1 0) system.

1.4.2. Bimetallic particles in highly dispersed systems

During the last two decades the main concern in the field of bimetallic catalysis was what happens if a mixture of two metals is deposited onto an *inorganic oxide support* forming thereby a highly dispersed catalyst. What additional effects can be observed due to the dispersion, which differ from the rules established for an alloy?

First, if the particle size decreases to the range characteristic of a cluster size (ca. 50 metal atoms), the electronic structure is altered. UPS studies have shown [36,37] that for Cu and Ag clusters the UPS band is narrowed and a shift in the d-threshold towards the Fermi energy occurs in the range of 2–150 atoms. Above this size, the spectra correspond to those characteristics of a bulk metal. With bimetallic systems [19], addition of IB metals to group VIII metals results in a band narrowing and with some metals (e.g. Pd/Ag) a d-band filling of the transition metal. In addition, a decrease in particle size tends to decrease the miscibility gap for metal pairs, which cannot form solid solutions [38].

Ponec [13] has listed some effects due to the diminished particle size. One of them is the change in electron structure, which is revealed in photoelectron spectroscopic properties. The local density of states spectra for small metal particles are indeed different from those measured in bulk [39–41], and this may have a dramatic effect on the reactivity of the active metal atoms. By decreasing the particle size there is a shift in binding energy in the valence band (UPS) and the core level photoelectron (XPS) spectra towards higher binding energy values can be observed ([13] and references therein). There are two reasons for this effect. One is the so-called 'initial state effect', which indicates a change in electron density due to the electron transfer between the components of the bimetallic system. When attraction between the ejected electron and the positive hole left behind decreases the kinetic energy of the electrons, it is called 'final state effect'. This is due to the small size of the particles; the absence of free relaxation of the electrons around the positive hole, which results from the different population of d-orbital and the different LDOS.

As was shown at high dispersion, the role of the second metal is different because of the narrowing of the d-bands (smaller probability of overlapping). Conversely, metallic dispersion can also be modified by the addition of a second metal. Here, three cases can be distinguished:

(i) Formation of a *mixed oxide phase*, in which the surface mobility of both metals is mutually prevented. This results in the formation of small oxide particles ultimately leading to the increased dispersion of the active metal component.

(ii) Another alternative is the formation of an *oxide interface between the support and the active metal*, which again leads to a stabilization of the high dispersion. The consequence of the enhanced dispersion is an increase of the defect sites, kinks, steps, edges and corners where the number of next neighbors decreases. Here again one can predict a narrowing of the LDOS at the Fermi level and a decrease in the overlapping of the metal d-orbitals with $2\pi^*$ antibonding orbitals e.g. in the CO molecule, which results in a weakening bond between the metal and the carbon atom. Furthermore, there is also an impact on the hydrogen bond strength, because multi-coordination of the s-type orbital is favored at low valence occupation [42].

(iii) The third effect of increased metal dispersion is diminished deactivation of supported metal catalysts [43]. Since on small particles the formation of a large carbide phase is not produced, in bimetallic particles

dilution of the active metallic component with a non-active metal decreases the ensemble size [44]. Furthermore, enhanced amounts of weakly bound surface hydrogen also retard the surface deactivation processes.

The presence of an inert material such as a catalyst carrier, of course, may further modify a bimetallic system. In some cases (e.g. Pt–Re and Pt–Sn), the metal–metal interaction cannot be established with certainty [45,46], because due to the presence of coordinatively unsaturated sites (CUS) on the support—the reduction of one of the components to the metallic state is hampered. That is, in some cases metal crystallites or particles are anchored to metal ions stabilized by oxide on the surface (e.g. Fe–Fe^{2+}–MgO system [47]). The presence of metal ion species on the surface, as a consequence of a strong metal support interaction (SMSI), may further strongly influence the electronic properties of a metal particle and the ensemble size. Conversely, stabilization or destabilization of the small metal particles in bimetallic catalysts can be influenced by using different supports [48].

2. Case studies

Although our knowledge about bimetallic catalysis has extended during the last decades, unified and comprehensive theory still does not exist. While the operative mechanism for systems having well-developed alloy phase, is more or less predictable, the major problem still underlies when there is a size decrease, such as in the range of nano-particles. Short-range ordering causes conflicting phenomena because diminishing particle size is always associated with decreasing metal loading on supported catalysts. When the metal particle size decreases, i.e. at high dispersion several side effects is developed, the following effects or their combination appears:

(i) Change of the LDOS and the electron binding energies. This strongly affects electron transfer between the two metals as well as the chemisorption bond strength between the metal surface and the substrates;
(ii) Increasing 'dangling' bonds at the metal particle surface, consequently changing the chemisorption;
(iii) Strong metal/oxide interaction (SMSI) with limited reducibility of one metal, or conversely, if one component is noble metal, it may facilitate the reducibility of the less noble metal;
(iv) In some cases the formation of bimetallic nano-particles is questionable.

2.1. Pd–Fe/Cab–O–Sil [49–57]

Several years ago palladium was introduced as an active catalyst for methanol formation in particular, when it was supported on alumina promoted by lanthanum [49]. It was also demonstrated that addition of small amount of iron in form of oxide or in ionic form to palladium increases the selectivity towards higher alcohol formation [50]. Characterization of PdFe/Cab–O–Sil catalyst by Mössbauer spectroscopy [51] at different Fe/Pd ratio formation of high spins Fe^{2+}, PdFe alloy and α-iron was observed. A comparison of the relative intensities of Fe^{2+}, PdFe alloy and α-iron with the catalytic activity demonstrates a correlation between the methanol activity and PdFe alloy formation. The maximum in methanol formation is around 16 at.% iron. At higher Fe/Pd ratio methanol activity is strongly suppressed and the catalyst becomes a traditional FT catalyst due to the presence of α-iron. The maximum in methanol formation was associated with the superimposing the effect of increasing PtFe alloy and the strong suppression of the H/Pd ratio due to the increasing amount of iron. Similar findings were observed for PtFe [52] and for IrFe catalyst at high pressure [53]. In both cases, alloy formation was associated with methanol activity, although in some cases it was not true [54].

As a possible explanation of this generalized phenomenon one can assume a shift in electron density, which is due to a rehybridization of d-electrons in the alloy resulting in a screening effect at the iron nucleus [55]. This influences the electron density responsible for the electron transfer to $2\pi^*$-antibonding orbital in the CO molecule (see Scheme 1). Thus, the metal–carbon bond strength diminishes and dissociation of the CO, which takes place on pure Pd [49], is suppressed, thereby hydrogenation of the C–O bond toward methanol is promoted.

The efficiency in methanol formation increases when the particle size decreases, for instance, when the bimetallic particles are encapsulated into a zeolite supercage [56,57]. In Fig. 2, the activity of methanol formation measured over $PdFe/SiO_2$ and PdFe/NaX samples as a function of iron concentration is plotted and on both catalysts a maximum was observed [57]. The Pd nano-particles in zeolite are more sensitive for the iron than those in the silica-supported bimetallic catalyst, this is why the maximum in activity is shifted towards smaller Fe/Pd atomic ratio.

2.2. Pt–Co/Al_2O_3 and Pt–Co/NaY systems

This is a well-defined system and the selectivity of CO hydrogenation to form methanol (or higher alcohol) or

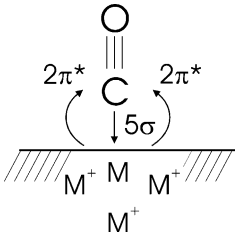

Scheme 1.

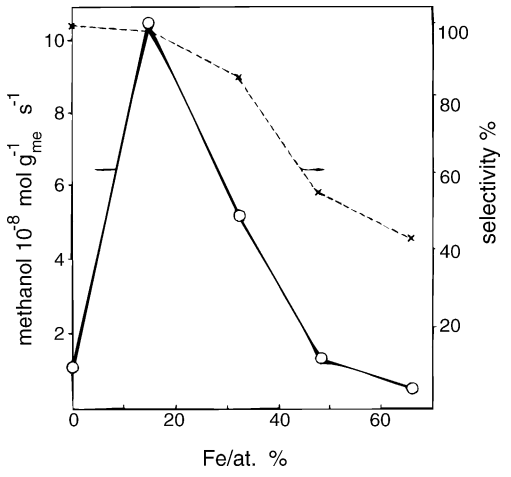

Fig. 2. Activity in methanol formation in the CO hydrogenation over PdFe/SiO_2 and PdFe/NaX samples [57].

hydrocarbons, largely depends on the particle size. Second, platinum is not just a modifier to facilitate cobalt reduction, but strongly affect the selectivity, too. Earlier and recent studies indicated that cobalt could not be reduced when the bimetallic sample is supported on alumina because a *cobalt surface phase* (CSP) is formed in a quasi-monolayer coverage [58–60] regardless of the metal loading. However, in the case of NaY zeolite both the TPR measurements and the EXAFS show a complete reduction of the cobalt ions. In Fig. 3, the TPR curves [61] are shown for the various Pt–Co samples. In the latter case, the particle size is around 1 nm and the selectivity is shifted towards the formation of oxygenates as shown in Table 1. We are confident that both on Al_2O_3 and NaY bimetallic particles are formed, but in the case of zeolite small particles are stabilized inside the zeolite supercage, whereas on the impregnated sample no oxygenates are formed.

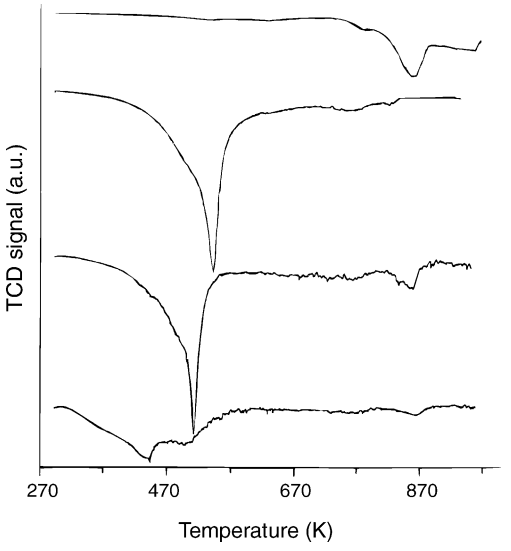

Fig. 3. Temperature-programmed reduction (TPR) of Pt/NaY (lower curve), Co/NaY (upper curve) and various Pt–Co/NaY samples [61].

Table 1
CO hydrogenation over PtCo/NaY samples prepared by ion exchange at 505 K and 10 bar

Catalyst	Rate[a]	CH_4	C^{2+}	CH_3OH	Oxygenate (%)[b]
PtCo/NaY[c]	27.9	27.3	17.3	50.4	5.0
PtCo/NaY[d]	16.5	42.9	28.8	20.6	7.7
Pt/NaY	15.0	41.2	27.2	26.3	5.3

[a] $\times 10^8$ mol s^{-1} g_{cat}^{-1}.
[b] Oxygenates other than methanol.
[c] Treatment: calcination at 573 K for 2 h and reduced at 723 K overnight.
[d] Oxidation at 573 K for 2 h and reduced at 723 K for 2 h after treatment (c).

The EXAFS studies using Pt L_{III}-edge and Co K-edge fully support the findings. After reduction in a stream of hydrogen results in metallic cobalt and platinum species formed [62]. The original sample presents an average coordination number of 6 for Co–O ($N_{CoO} = 6.0$, $R_{CoO} = 2.08$ Å). The metallic reference and the catalyst exhibit very similar shape in the XANES part, while a shift in the maximum of the FT module toward long distance is measured. Thus, we assume that the crystallographic network of the metallic particles and of the metallic reference is the same. Numerical simulations quantify this appearance of Co–Co metallic bonds ($N = 7.7$, $R = 2.50$ Å).

After being exposed to air, the Co environment still consists of Co atoms. This surprising structural result points out the presence of metallic species inside the catalyst particles. Nevertheless, a significant decrease of the Co–Co coordination number is revealed being 5.9 (instead of 7.7), leaving the interatomic distance unchanged ($N = 5.9$, $R = 2.51$ Å).

At the initial state the Pt L_{III}-edge indicates Pt–O bonds as shown by the large white line measured at the edge (Fig. 4) as well as the position and the shape of the Fourier transform module (Fig. 5). The numerical simulations performed for the EXAFS oscillation lead to a number of 4.4 O-atoms at 2.05 Å.

After the in situ reduction, Pt–O bonds are broken and replaced by Pt–Co bonds as shown by the decrease of the white line intensity and the shift toward the long distance of the Fourier transform module. Numerical simulation indicates that only Pt–Co bonds are formed. The different values of the structural parameters are for the coordination number $N_{Pt–Co} = 5.4$ and for the interatomic distance $R_{Pt–Co} = 2.57$ Å.

Finally, the air exposure to the sample modifies significantly the local order around Pt atoms. Part of the Pt–Co bonds disappear ($N_{Pt–Co} = 2.5$ instead of 5.4, $R_{Pt–Co} = 2.52$ Å) while an oxidation process of Pt is observed ($N_{Pt–O} = 1.0$, $R_{Pt–Co} = 2.06$ Å). Cubo-octahedra model calculation the maximum diameter can be estimated for the bimetallic particles to be 1.5 nm.

The CO hydrogenation provides supporting evidence for stability of the bimetallic particles. During long-time on-stream, the catalytic activity and selectivity remain relatively constant [63], which indicates the presence of the bimetallic particles. In rows 2 and 3 of Table 1 the catalytic

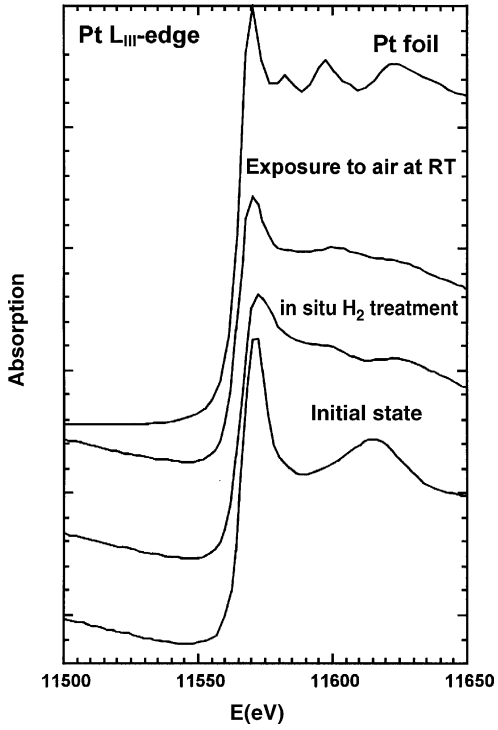

Fig. 4. XANES part of Pt L_{III}-edge in Pt–Co/NaY sample after various treatments [69].

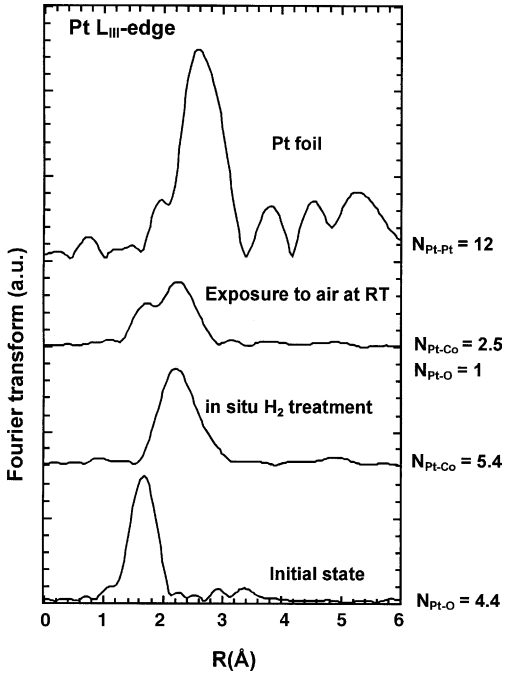

Fig. 5. Fourier transform of Pt L_{III}-edge after various treatments [62].

activities and selectivity are given for a Pt–Co/NaY sample in which the two metals were separated after oxidation (the Pt particles are localized in the supercages) and for a Pt/NaY sample, respectively. In both cases, methane selectivity increased and oxygenates selectivity decreased in comparison with the Pt–Co/NaY sample (row 1) indicating that the PtCo/NaY catalyst after reoxidation becomes similar to the Pt/NaY sample.

The above example clearly shows that once Pt–Co bimetallic particles have been formed, separation occurs after mild oxidation at 570 K leaving Pt particles in the zeolite supercage. However, we also have to prove whether or not migration to the external surface occurs. In order to mimic the segregation of the metals to the external surface, two different Pt–Co/NaY samples were compared prepared by either ion exchange (IE) or by incipient wetness impregnation (IM). The particle size for IE and IM are $S < 2.5$ and 20 nm, respectively [64]. The data on the CO hydrogenation are shown in Table 2. As appears from Table 2, when small bimetallic particles are formed and located inside the supercage of the NaY zeolite (IE), the oxygenate selectivity is high. On the other hand, if the particles had migrated out of the supercage to form large particles at the external surface of the zeolite (IM), the catalyst would work as a platinum-promoted cobalt catalyst with no oxygenate selectivity and large amount of C^{2+} hydrocarbons.

2.3. Ru–Co/NaY samples

In the Ru–Co/NaY samples, the presence of bimetallic particles was evidenced by repeated oxidation/reduction cycles in which Co^{2+} ions were always reduced into metallic state after hydrogenation due to the intimate contact between cobalt and ruthenium. This was first evidenced by TPR and XPS measurements [65,66].

The reducibility of the samples depends on the size of the metal particles. For instance, when the Ru^{3+} ions are reduced after helium treatment, reduction is not complete, but the size of metal particles is small indicated by CO chemisorption [67]. Quite normally Co^{2+} ions are reduced at high

Table 2
Comparison of Pt–Co/NaY samples (IE and IM) in the CO hydrogenation measured at 1 bar pressure

Catalyst	T (K)	Rate[a]	CH_4 (%)	C^{2+} (%)	Olefin (%)[b]	MeOH (%)	Oxygenate (%)[c]
PtCo/NaY (IE[d])	502	0.35	78.7	8.0	0	0	13.3
PtCo/NaY (IM[e])	505	0.69	53.6	46.4	16.1	0	0

[a] $\times 10^{-4}$ mol s^{-1} mol^{-1}_{metal}.
[b] Olefin selectivity in C^{2+} hydrocarbons.
[c] Oxygenates other than methanol.
[d] Ion exchanged.
[e] Impregnated.

Table 3
The activity and selectivity of Co/NaY, Ru/NaY and Co–Ru/NaY catalysts (1 g catalyst, H_2/CO/Ar molar ratio of 6:3:1); T = 502 K; p = 21 bar

Catalyst	X (%)	C%					
		CH_4	C_2–C_4	C_5–C_8	$>C_8$	Oxygenate	CO_2
Co/NaY	1.1	44	37	15	7	0	0
Ru/NaY	86	75	1.1	0.5	0	0	23
Co–Ru/NaY	9	26	35	22	16	0.4	0

temperature to a small extent, however, their reducibility is greatly affected by the addition of ruthenium.

The activity of the Ru/NaY, Co/NaY and Co–Ru/NaY samples were measured in the CO hydrogenation at 21 bar in the temperature range between 463 and 563 K. The results presented in Table 3 show that the steady-state activity in the CO conversion at 507 K increases in the sequence of Co/NaYS < Ru–Co/NaYS < Ru/NaY, which indicates a promoting effect of ruthenium for cobalt. Over the Co-containing samples no CO_2 is formed and the main difference lies in the activity being the Ru–Co/NaY sample 10-fold more active than the pure Co/NaY [67].

Although the XPS and TPR results points to the formation of bimetallic particles inside the NaY supercage (see Table 4), the EXAFS results do not support the presence of bimetallic particles (indeed, metallic cobalt is formed in the oxidation/reduction cycle) [68,69].

In Fig. 6, the modules of the Fourier transform associated with the metallic cobalt foil (curve e) and the reduced Ru–Co/NaY sample (curve b). From these spectra, the number of cobalt atoms in the first coordination sphere, $N_{Co–Co}$ = 7.0, their distance, $R_{Co–Co}$ = 0.2509 nm. This clearly shows the presence of Co–Co metal bonds. Drastic decrease in the coordination number (from 12 for Co foil to 7.0 in zeolite) is due to the fact that in zeolite the cobalt atoms are in the form of metal nano-cluster.

In Fig. 7 the absorption spectrum of XANES part of the Ru K-edge measured in the Ru–Co/NaY sample is shown. The shape of the curve due to the reduced sample is very similar to that measured on Ru metallic foil. The numerical simulation confirmed this qualitative estimation of the environment of ruthenium.

After reduction a lower coordination number ($N_{Ru–Ru}$ = 4.9) was recorded for ruthenium than for cobalt. This may indicate that ruthenium is located near to the cobalt surface. Surprisingly, no signal characteristic of the Co–Ru heteroatomic bond seems to be present inside the material as

Table 4
XPS measurements on Ru–Co/NaY

Treatment (K/gas/h)	Ru 3p (BE/eV)	Co 2p (BE/eV)	Co species
As-received	463.5 (0.51)	781.7 (2.28)	
573/He/2	463.0 (0.65)	781.6 (2.44)	
723/H_2/2	461.3 (0.42)	777.9 (1.40)	←Co^0
573/O_2/2	463.0 (0.37)	780.0 (1.55)	
723/H_2/2	460.4 (0.43)	777.4 (1.41)	←Co^0

The Ru 3p/Si 1s and Co 2p/Si 1s ratio are given in parantheses.

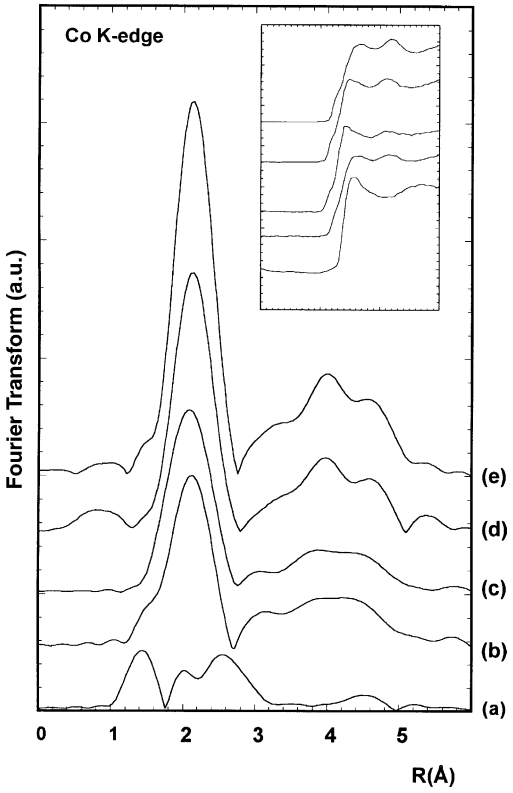

Fig. 6. Fourier transform at the Co K-edge for the Ru–Co/NaY catalyst in as-prepared state (a), after reduction (b), after air exposure (c), spent catalyst (d) and metallic cobalt foil (e) as reference. Inset: XANES part for the same treatment [62].

confirmed by the numerical simulations (the Co environment refined from the EXAFS of the Ru–Co bimetallic catalyst). Only Co–Co and Ru–Ru bonds are formed after hydrogen treatment.

The XPS results on the Ru–Co/NaY samples indicated the reduction/oxidation cycles to be a reversible process [4]. That is, the role of ruthenium is to promote the reduction of Co^{2+} ions thereby increasing the number of metallic cobalt atoms in zeolite. From the XPS data it was not unambiguously proven whether this reversibility is attributed to alloy formation inside the NaY supercage. The lack of Ru–Co bonds found by EXAFS suggests that either the concentration of the alloy species is under the analytical limit, or separate cobalt and ruthenium nano-particles are present in close vicinity to each other. We may speculate whether or not during preparation of the bimetallic sample by treatment in hydrogen the Ru metal particles – after supplying hydrogen atoms for reduction of cobalt – decorate the cobalt nano-particles. If the decoration does not result in alloy formation, but in a sort of physical interaction, the lack of Ru–Co bond may be understood. Nevertheless, Co^{2+} ions still exist in the sample due to the partial reduction. These ions may retard migration of the metal atoms in the interior of the zeolite or to its external surface.

Quite surprisingly after air exposure metallic Co–Co bonds still exist inside the zeolite despite the high reactivity

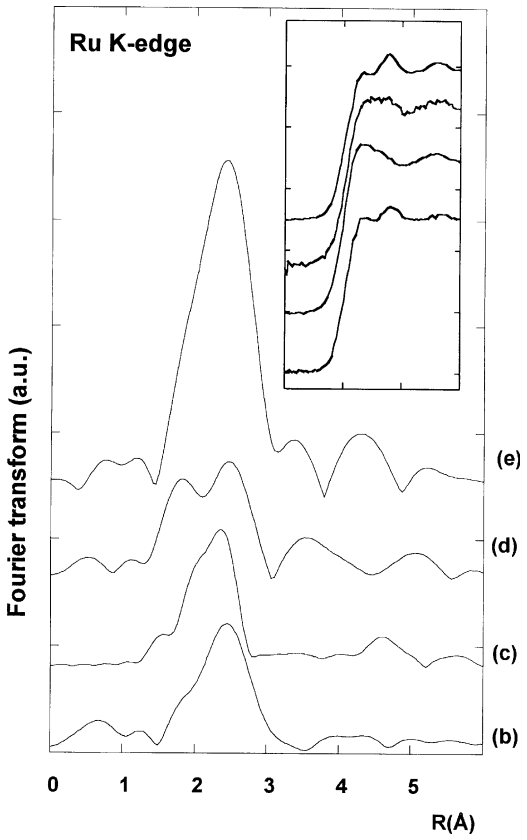

Fig. 7. Fourier transform at the Ru K-edge for the Ru–Co/NaY catalyst. For notation see Fig. 5 (the top curve is Ru metallic foil). Inset: the XANES part of the various treatments [68].

of Co to oxidation. Regarding the second metal, we observe the formation of Ru–O bonds and the number of Ru–Ru decreases significantly. These experimental findings support the picture described above for the chemical nature of bimetallic phase in zeolite.

The *scenario* put forward previously in the CO hydrogenation can also be slightly modified. The production of short chain hydrocarbons and low olefin/paraffin ratio [67,70,71] was explained by hydrogenolysis in the pores containing Ru–Co particles in the NaY sample. In the light of the present results, we incline to attribute the short chain hydrocarbons observed to intensive hydrogenation on the ruthenium decorating the cobalt particles. Thus, whilst leaving the supercage, the olefins leading to higher hydrocarbons by re-adsorption, are competitively hydrogenated to produce paraffins resulting in low olefin/paraffin ratio. These catalytic results strongly support the features of the Ru–Co/NaY system obtained by physical methods.

The EXAFS results have certain, but not irresolvable contradiction to the in situ XPS measurements, by which we suggested the presence of bimetallic Ru–Co particles inside the NaY zeolite [65]. EXAFS measurements highlight the fine structure, i.e. ruthenium is more accessible to the reacting substrates in the bimetallic particles than Co. Consequently, ruthenium may decorate the cobalt surface and/or being in its close vicinity. The catalytic measurements in the CO hydrogenation give evidence of the above structure [71]. The Ru–Co/NaY samples have the same rate, temperature dependence of the Schulz–Flory distribution and the olefin/paraffin ratios regardless of the pretreatments.

To sum up, when the particle size is in the range nano-size, careful analysis is needed to determine the existence of bimetallic particle [72], its stability and restructuring (maybe disintegration). If the two monometallic nano-particles are in the intimate contact the reversible oxidation/reduction can take place, but this is not a sole indication of bimetallic nano-particles.

2.4. Gold system

Gold is one of the most curious metal, which has no catalytic activity in the form of large particles, whereas its activity is extremely high when it is present in form of nano-particles. There has been a large effort to substitute platinum with gold, as the price is the lowest among the Pt metals. Platinum is one of the most frequently applied catalysts for hydrocarbon reactions; it is therefore not surprising that its modification has long been a subject for research. The modification of platinum using group IB and other transition metals (Au, Cu, Pd, Ir, Ru and Fe) has been reviewed elsewhere [73].

2.5. Platinum–gold

Alloying gold with platinum is one of the typical examples that show ensemble size effect [74]. In agreement with the theory given by van Santen [75], on increasing the Au concentration, CO adsorption takes place preferentially in an on-top position instead of in the valley between two Pt atoms. Au addition can control the ensemble size, as shown in the dehydrogenation of cyclohexane (with small ensembles cyclohexene appears as an intermediate as a consequence of the step-wise dehydrogenation mechanism) [76]. However, as a side effect, on small Pt ensembles all self-poisoning reactions are retarded, as indicated by the enhanced rate of isomerization of *n*-hexane. Surface coverage with hydrogen can also be influenced by alloying. Propane dehydrogenation requires two adsorption sites located on one platinum atom [77]. The mechanism of propane dehydrogenation is the same for Pt and Pt–Au alloys, but the TON is higher for platinum itself than for alloys. This fact, along with the reaction order with respect to hydrogen, suggests the depletion of hydrogen surface coverage on alloys. By supporting the Pt–Au system (16 wt.% metal) no drastic change can be seen compared to alloy film or powder [78]. Diluted platinum (1–4 at.%) catalyses *n*-hexane and *n*-pentane isomerizations by a one-site mechanism, i.e. Pt activity is not influenced by the surrounding Au atoms, 10 at.% Pt favors dehydrocyclization

due to the larger ensemble size, whereas pure platinum isomerizes *n*-hexane mainly via a bond-shift mechanism. Apparently no segregation occurs, unlike the highly dispersed silica-supported PtAu catalyst with low metal loading (0.7 wt.%) where separate Au particles are present along with Pt–Au bimetallics [79]. The ensemble size effect principle is also valid here because, in the hydrogen transfer reaction between benzene and cyclohexane, Au atoms as diluent change the ensemble size of platinum. However, at higher metal loadings the reaction rate is increased by increasing gold addition; this effect may be due – unlike the explanation given by the authors – to inhibition of the poisoning reaction. Surface enrichment of gold after thermal treatment seems to be a general phenomenon. For a series of Pt–Au bimetallic systems supported on different carriers with 1 to 2 wt.% metal loading, the TPD profile of adsorbed hydrogen was seen to be independent of gold content [80] as a consequence of the equilibrium gold coverage. If the silica support is changed for an alumina carrier, the SMSI may not be ruled out [34]. The Al_2O_3 and SiO_2-supported Pt–Au catalysts after two oxidation–reduction cycles behave differently (see Fig. 2). As shown, SiO_2-supported Pt–Au does not change its activity and selectivity, whereas the Al_2O_3-supported bimetallic catalyst does. A possible explanation, given by de Jongste and Ponec [81], is that upon oxidation, segregation occurs on the alumina-supported catalyst and the bimetallic particle disintegrates to small Pt particles and large Au crystallites. Consequently, cyclization, which requires a single site, increases compared to isomerization. Obviously, the effect of the addition of gold to platinum can be explained by the change of ensemble size as the major reason, with some marginal effects of surface hydrogen coverage, retardation of self-poisoning reactions, and strong metal–support interaction (SMSI) [81].

2.6. Palladium–gold nano-particles on SiO_2

The interest in the use of gold in heterogeneous catalysis has recently increased on the basis of experimental evidences of its surprisingly high activity in the low temperature oxidation of CO [82]. To this respect, the support materials play an important role in the catalytic behaviour of this metal. The supports, generally being metal oxides, are divided into two categories: the active supports, such as the reducible Fe_2O_3, TiO_2 and Co_2O_3, and the inert supports, such as SiO_2, Al_2O_3 and MgO [83].

The catalysts supported on active oxides exhibit superior activity attributed to their ability to provide reactive oxygen [83], most likely oxide vacancies are formed near to the gold/support interface offering a site for oxygen adsorption [84,85]. These sites are abundant in the proximity of the gold particles. Therefore, the sites along the perimeter of gold/support interface would be the favourite sites for the reaction between CO adsorbed on Au and the oxygen adsorbed on the support.

The achievement of small particle size is not always an easy task and many experimental variables play major role. Particularly, in the case of gold catalysts, reproducibility of catalytic results is rarely accomplished. The reason for this failure is the sensitivity of the catalyst surface to pre-treatment and to reaction conditions.

The use of bimetallic catalysts can be a way to limit such dependence, by increasing the resistance to particle sintering. Moreover, alloying with a second metal allows changing the geometry and the electronic properties of the active site in such a way to achieve the effect of the particle size variation [5,7]. Furthermore, recent studies have shown superior activities of supported alloyed gold–palladium catalysts in different type of reactions such as in the hydrodechlorination of chlorofluorocarbons (CFCs) [86], and in the hydrodesulfurization reaction [87].

The choice of palladium as a second metal is dictated by its well-recognised activity in this type of reaction [88]. By adopting a preparation procedure using a colloidal solution of metal particles, a series of silica-supported Au–Pd catalysts with different Au/Pd atomic ratios were prepared. Silica was used as support because of its inert character, which would allow to investigate the reciprocal effects of the two metals without interference from metal–support interaction. The catalysts were characterized by several techniques. X-ray diffraction (XRD), X-ray photoelectron spectroscopy (XPS), temperature-programmed reduction (TPR), transmission electron microscopy (TEM) and chemisorption of CO. Bimetallic Au–Pd catalysts supported on silica with different Au/Pd atomic ratios were prepared by simultaneous reduction of palladium and gold precursors by ethanol in the presence of the polymer, polyvinylpyrrolidone (PVP). The formation of alloyed particles was detected by means of X-ray diffraction (shown in Table 5). The catalysts were tested in the catalytic oxidation of CO using a plug-flow reactor. The CO conversion as a function of temperature was determined as shown in Fig. 8. The monometallic palladium and the palladium-rich catalysts behaved quite similarly and were the most active catalysts. A drastic reduction of the CO oxidation activity was observed for the 50/50 Au/Pd catalyst and for samples with increasing amount of gold (see Table 6).

Table 5
Crystal phases of the mono- and bi-metallic samples with the relative molar percentages after calcinations at 673 K

Catalyst	Crystal phases (size in nm) %
Pd/SiO_2	PdO (10.5) 98%, Pd (39) 2%
$10Au–90Pd/SiO_2$	PdO (9.6) 95%, Au_6Pd_{94} (7.3) 5%
$25Au–75Pd/SiO_2$	PdO (8) 78%, $Au_{43}Pd_{57}$ (4.2) 22%
$50Au–50Pd/SiO_2$	PdO (8.7) 19%, $Au_{52}Pd_{48}$ (3.7) 81%
$50Au–50Pd/SiO_2$(II)[a]	PdO (10.4) 18%, $Au_{47}Pd_{53}$ (3.9) 82%
$75Au–25Pd/SiO_2$	$Au_{62}Pd_{38}$ (4.5) 100%
$90Au–10Pd/SiO_2$	Au (27.5) 24%, $Au_{87}Pd_{13}$ (7) 76%
Au/SiO_2	Au (32) 100%

The corresponding crystal particle sizes are given in parentheses.
[a] Second preparation.

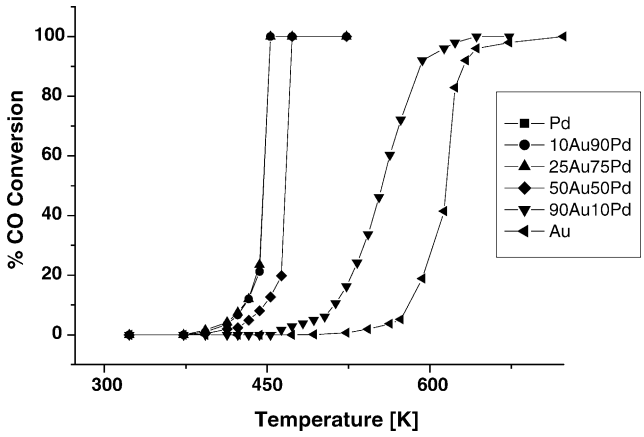

Fig. 8. Conversion of CO vs. temperature on $AuPd/SiO_2$ samples: 50 mg catalysts; 50 ml/min gas mixture (4500 ppm CO + 5000 ppm O_2) [90].

The catalytic results from the present series of catalysts indicate that in the absence on any support–metal interaction as for the silica case, gold catalysts are much less active than palladium catalysts. The poor activity for the silica-supported gold catalyst can be attributed to the large sizes of the gold particles. The alloying with palladium atoms, although determines a decrease in the particle size, does not contribute to the activity increase. Furthermore, the effect of gold in inhibiting the oxidation of Pd during the probe reaction could be responsible for the observed decrease of activity [89].

2.7. Palladium–gold nano-particles on TiO_2

In contrast to Pd–Au/SiO_2 the titania-supported bimetallic catalysts are more active. As shown in Table 7 not only

Table 6
Catalytic results in terms of CO conversion, reaction rates and turnover frequencies

Catalysts	$CO_{conv.}$ (%)	r_0 (μmol min^{-1} g_{cat})	D_{XRD}	TOF_{XRD} (min^{-1})	D_{CO}[a] (%)	TOF_{CO} (min^{-1})
Pd/SiO_2	5.1	9.3	11	0.59	11.6 (1.9)	0.56
10Au–90Pd/SiO_2	3.5	6.4	12	0.44	15.3 (1.8)	0.35
25Au–75Pd/SiO_2	4.2	7.7	16	0.40	16.8 (1.7)	0.38
50Au–50Pd/SiO_2	2.0	3.6	24	0.24	16.5 (1.2)	0.36
90Au–10Pd/SiO_2	0	–	16	–	–	–
Au/SiO_2	0	–	–	–	–	–

Palladium dispersion calculated from XRD and from CO chemisorption is also reported.
[a] Assumed Pd/CO ratios are in parentheses.

Table 7
Metal loading, crystalline phases, particle size and the estimated concentration of surface metal atoms in the supported samples

Sample	As-prepared state				Calcined/reduced state		
	Au (wt.%)	Pd (wt.%)	XRD phases (size nm^{-1})	XRD phases[a] (size nm^{-1})	d_{TEM} (nm) (μmol g_{cat}^{-1})	$M_{surface,TEM}$ (μmol g_{cat}^{-1})	$Pd_{surface,CO}$
$AuTiO_2$	1.95	–	Au (8)	Au (8)	12.9 ± 5.9	9.0/Au	–
$PdTiO_2$	–	1.10	Pd (4)	Pd (8)	8.8 ± 3.6	13.2/Pd	18.8
$AuPdTiO_2$	1.08	0.55	Au75Pd25 (5)	Au75Pd25 (8)	9.6 ± 4.0	6.2/Pd, 6.5/Au	17.0
Au/SiO_2	0.73	–	–	Au (32)	95.1 ± 28	0.46/Au	–
Pd/SiO_2	–	0.53	–	PdO (10) 98%, Pd (4) 2%	9.2 ± 3.6	17.5/Pd	16.7
50Au–50Pd/SiO_2	0.65	0.63	–	PdO (9) 19%, Au52Pd48 (4) 81%	6.2 ± 2.1	11.1/Pd, 5.8/Au	10.1

Concentration of surface Pd atoms calculated from CO chemisorption; no CO chemisorption was detected on the monometallic Au samples.
[a] XRD was measured on the calcined form of the SiO_2-supported samples.

Table 8
Comparison of the activity of SiO_2- and TiO_2-supported gold palladium samples

Samples	Temperature (°C)	Initial reaction rate (μmol min^{-1} g_{cat}^{-1})	TOF_{XRD} (min^{-1})	TOF_{TEM} (min^{-1})	TOF_{CO} (min^{-1})
Au/TiO_2	60	12.1	0.84	1.35	–
Pd/TiO_2	60	13.7	0.95	1.04	0.73
66Au–34Pd/TiO_2	60	22.9	–	–	–
Au/SiO_2	220	0.16	–	0.36	–
Pd/SiO_2	140	9.3	0.59	0.53	0.56
50Au–50Pd/SiO_2	140	3.6	0.24	0.32	0.36

small gold nano-particles can be stabilized by TiO_2, but calcination/reduction does not alter the size, either. In Table 8 the activity of bimetallic titania-supported samples are compared with silica-supported ones. In the latter case slight synergism is experienced as reported earlier [90].

3. Conclusions

The paper featuring bimetallic catalysts concerns with the effect of these catalysts on the reactivity and selectivity. The key issue is that normally the two metals – if alloy is formed – do not lose their identities but overlapping the d-bands affects the valence state of the metal atoms. In some cases the miscibility gap is so large that alloy is not formed, in this case one of the components is less reducible than the other (e.g., noble metals) and the interaction of the former with the support may stabilize the highly dispersed state of the noble metal component.

Conversely, the addition of the noble metal to the hardly reducible component facilitates the reduction, which causes the retardation of the deactivation process of some hydrocarbon reaction.

The effect is more pronounced when the particle size decreases, for instance, when the metal particles are inserted into zeolite matrix and the metal particles in nano-scale range. In Section 2, we illustrated how the change of the electron density in the valence state may alter the mode of CO chemisorption from dissociative to associative form, increasing thereby the alcohol formation in the CO hydrogenation. Furthermore, selective hydrogenation as an example was also discussed.

Acknowledgements

The author is indebted to the National Science and Research Fund for financial support (Grant nos.: T-034920 and T-022117). The support of the COST 15 program (Grant no.: COST D15/0005/99) is also acknowledged, in particular, the author is grateful to Dr. D. Bazin who arranged the EXAFS experiments in LURE, Orsay, published elsewhere. The author gratefully acknowledges the help of Dr. Z. Schay, Dr. L. Borko, Dr. A. Beck, Dr. A. Horvath and Ms. K. Frey.

References

[1] D.A. Dowden, P.W. Reynolds, Disc. Faraday Soc. 8 (1950) 184.
[2] T. Takeuchi, M. Sakaguchi, I. Miyoshi, T. Takabatake, Bull. Chem. Soc. Jpn. 35 (1962) 1390.
[3] D.F. Ollis, J. Catal. 23 (1971) 131.
[4] H.C. de Jongste, V. Ponec, Bull. Soc. Chim. Belg. 88 (1979) 453.
[5] W.H.M. Sachtler, R.A. van Santen, Adv. Catal. 26 (1977) 69.
[6] W.H.M. Sachtler, R.A. van Santen, Appl. Surf. Sci. 3 (1979) 121.
[7] W.H.M. Sachtler, in: R. Prins, G.C. Schuit (Eds.), Chemistry and Chemical Engineering of Catalysis Processes, Sijthoff & Noordhoff, The Netherlands, 1980, p. 317.
[8] V. Ponec, in: R. Prins, G.C. Schuit (Eds.), Chemistry and Chemical Engineering of Catalysis Processes, Sijthoff & Noordhoff, The Netherlands, 1980, p. 257.
[9] H.C. de Jongste, V. Ponec, in: R. Prins, G.C. Schuit (Eds.), Chemistry and Chemical Engineering of Catalysis Processes, Sijthoff & Noordhoff, The Netherlands, 1980, p. 337.
[10] H.C. de Jongste, F.J. Kuijers, V. Ponec, in: B. Delmon, P.A. Jacobs, G. Poncelet (Eds.), Preparation of Catalysts, Elsevier, Amsterdam, 1976, p. 207.
[11] V. Ponec, Surf. Sci. 80 (1979) 352.
[12] M.W. Vogelzang, M.J.P. Botman, V. Ponec, Disc. Faraday Soc. 72 (1982) 33.
[13] V. Ponec, Adv. Catal. 32 (1983) 149.
[14] V. Ponec, G.C. Bond (Eds.), Catalysis by Alloys, Elsevier, Amsterdam, 1995.
[15] L. Guczi, A. Sárkány, Catalysis, in: J.J. Spivey (Ed.), Specialist Periodical Reports, vol. 11, The Society of Chemistry, London, 1994 (Chapter 8), p. 318;
L. Guczi, J. Mol. Catal. 25 (1984) 13;
L. Guczi, in: B.C. Gates, H. Knözinger, L. Guczi (Eds.), Metal Cluster in Catalysis, Elsevier, Amsterdam, 1986 (Chapter 10), p. 547.
[16] R.A. van Santen, W.H.M. Sachtler, J. Catal. 33 (1974) 202.
[17] R.A. van Santen, M.A.M. Boersma, J. Catal. 34 (1974) 13.
[18] S. Hüfner, G.K. Wertheim, J.A. Wernick, Phys. Rev. B 8 (1973) 4511.
[19] J.H. Sinfelt, Acc. Chem. Res. 10 (1977) 15.
[20] J.K.A. Clarke, Chem. Rev. 75 (1975) 291.
[21] V. Ponec, in: E.G. Derouane, A.A. Lucas (Eds.), Electronic Structure and Reactivity of Solid Surfaces, Plenum Press, New York, 1976, p. 537.
[22] V. Ponec, Catal. Rev. Sci. Eng. 11 (1975) 1.
[23] L. Guczi, A. Frennet, V. Ponec, Acta Chim. Hung. 112 (1983) 127.
[24] R.A. van Santen, Rec. Trav. Chim. Pays-Bas 101 (1982) 121.
[25] S. Engels, W. Mörke, J. Siedler, Z. Anorg. Allg. Chem. 431 (1977) 191.
[26] U. Bardi, B.C. Beard, P.N. Ross, J. Catal. 124 (1990) 22.
[27] U. Bardi, A. Atrei, P. Ross, E. Zanazzi, G. Rovida, Surf. Sci. 211–212 (1989) 441.
[28] F. Boccuzzi, A. Chiorino, G. Ghiotti, F. Pinna, G. Strukul, R. Tessari, J. Catal. 126 (1990) 381.
[29] P. Pervan, M. Milun, Surf. Sci. 264 (1992) 135.
[30] J.W. He, W.L. Shea, X. Jiang, D.W. Goodman, J. Vac. Sci. Technol. 8 (1990) 2435.
[31] J.W. He, D.W. Goodman, J. Phys. Chem. 94 (1999) 1502.
[32] P.J. Berlowitz, D.W. Goodman, Surf. Sci. 187 (1987) 463.
[33] J.A. Rodriguez, D.W. Goodman, in: L. Guczi (Ed.), New Trends in CO Activation, Elsevier, Amsterdam, 1991 (Chapter 3).
[34] J.A. Rodriguez, R.A. Campbell, D.W. Goodman, J. Phys. Chem. 94 (1990) 6934.
[35] R.A. Campbell, J.A. Rodriguez, D.W. Goodman, in: L. Guczi, F. Solymosi, P. Tétényi (Eds.), Proceedings of the 10th International Congress on Catalysis, vol. A, Akadémiai Kiadó, Budapest, 1993, p. 333.
[36] R.C. Baetzold, Surf. Sci. 106 (1981) 243.
[37] R.C. Baetzold, J.F. Hamilton, Progress in Solid State Chemistry, vol. 15, Pergamon Press, New York, 1983, p. 1.
[38] B.S. Gudkov, P. Tétényi, L. Guczi, J. Catal. 74 (1982) 207.
[39] V. de Gouveia, B. Bellamy, A. Masson, M. Che, in: C. Morterra, A. Zecchina, G. Costa (Eds.), Structure and Reactivity of Surfaces, Elsevier, Amsterdam, 1989, p. 347.
[40] Masson, in: C. Morterra, A. Zecchina, G. Costa (Eds.), Structure and Reactivity of Surfaces, Elsevier, Amsterdam, 1989, p. 665.
[41] P. Legare, Y. Sakisaka, C.F. Brucker, T.H. Rhodin, Surf. Sci. 139 (1984) 316.

[42] R.A. van Santen, Faraday Symp. Chem. Soc. 21 (1986), 1.
[43] E.H. van Broekhoven, J.W.F.M. Schoonhoven, V. Ponec, Surf. Sci. 156 (1985) 899.
[44] F.J.C.M. Toolenar, V. Ponec, J. Catal. 83 (1983) 251.
[45] N. Wagstaff, R. Prins, J. Catal. 59 (1979) 434.
[46] P.S. Kirlin, B.R. Strochmeier, B.C. Gates, J. Catal. 98 (1986) 308.
[47] H. Topsoe, J.A. Dumesic, E.G. Derouane, B.S. Clause, S. Morup, J. Villadsen, N. Topsoe, in: B. Delmon, et al. (Eds.), Preparation of Catalysts, vol. 2, Elsevier, Amsterdam, 1979, p. 365.
[48] P. Turliers, J.A. Dalmon, G.A. Martin, in: B. Imelik, et al. (Eds.), Metal Support and Metal Additives Effects in Catalysis, Elsevier, Amsterdam, 1983, p. 203.
[49] J.M. Driessen, F.K. Poels, J.P. Hindermann, V. Ponec, J. Catal. 82 (1983) 26.
[50] T. Fukushima, K. Aradki, M. Ichikawa, J. Chem. Soc. Chem. Commun. 148 (1986).
[51] G. Lietz, M. Nimz, J. Völter, K. Lázár, L. Guczi, Appl. Catal. 45 (1988) 71.
[52] H.S. Woo, T.H. Fleisch, H.C. Foley, S. Uchiyama, W.N. Delgass, Catal. Lett. 4 (1990) 93.
[53] M. van der Kraan, H.A. Martens, J.W. S Niemantsverdriet, in: Proceedings of the 10th North American Meeting of the Catalysis Society, San Diego, May 17–24, 1987, p. D33.
[54] M.A. Vannice, R.L. Garten, J. Mol. Catal. 1 (1975) 201.
[55] L. Guczi, K. Matusek, M. Eszterle, J. Catal. 60 (1979) 121.
[56] K. Matusek, I. Bogyay, L. Guczi, G. Diaz, F. Garin, G. Maire, J. C1 Mol. Chem. 1 (1985) 335.
[57] L. Guczi, Catal. Lett. 7 (1990) 205.
[58] L. Guczi, I. Kiricsi, Appl. Catal. A 186 (1999) 375.
[59] Z. Zsoldos, T. Hoffer, L. Guczi, J. Phys. Chem. 95 (1991) 798.
[60] L. Guczi, T. Hoffer, Z. Zsoldos, S. Zyade, G. Maire, F. Garin, J. Phys. Chem. 95 (1991) 802.
[61] G. Lu, T. Hoffer, L. Guczi, Catal. Lett. 14 (1992) 207.
[62] L. Guczi, D. Bazin, I. Kovács, L. Borkó, Z. Schay, J. Lynch, P. Parent, C. Lafon, G. Stefler, Zs. Koppány, I. Sajó, Top. Catal. 20 (2002) 129.
[63] G. Lu, Z. Zsoldos, Zs. Koppány, L. Guczi, Catal. Lett. 24 (1994) 15; G. Lu, L. Guczi, in: H.K. Beyer, H.G. Karge, I. Kiricsi, J.B. Nagy (Eds.), Studies in Surface Science and Catalysis, vol. 94, Elsevier, Amsterdam, 1995, p. 171.
[64] L. Guczi, G. Lu, Z. Zsoldos, Zs. Koppány, Zeolites and related microporous materials: state of the art 1994, in: J. Weitkamp, H.G. Karge, H. Pfeifer, W. Hölderich (Eds.), Studies in Surface Science Catalysis, vol. 84, Elsevier, Amsterdam, 1994, p. 949.
[65] L. Guczi, R. Sundararajan, Zs. Koppány, Z. Zsoldos, Z. Schay, F. Mizukami, S. Niwa, J. Catal. 167 (1997) 482.
[66] L. Guczi, Z. Kónya, Zs. Koppány, G. Stefler, I. Kiricsi, Catal. Lett. 44 (1997) 7.
[67] L. Guczi, G. Stefler, Zs. Koppány, V. Komppa, M. Reinikainen, Science and technology in catalysis, in: H. Hattori, K. Otsuka (Eds.), Studies in Surface Science and Catalysis, vol. 121, Kodansha/Elsevier, Tokyo/Amsterdam, 1999, p. 209.
[68] L. Guczi, D. Bazin, I. Kovács, L. Borkó, I. Kiricsi, Stud. Surf. Sci. Catal. 136 (2001) 111.
[69] D. Bazin, I. Kovács, J. Lynch, L. Guczi, Appl. Catal. A 242 (2003) 149.
[70] L. Guczi, Zs. Koppány, K.V. Sarma, L. Borkó, I. Kiricsi, in: H. Chon, S.-K. Ihm, Y.S. Uh (Eds.), Studies in Surface Science and Catalysis, vol. 105, 1997, p. 861.
[71] G. Stefler, I. Kiricsi, L. Guczi, Porous materials in environmentally friendly processes, in: I. Kiricsi, G. Pál-Borbély, J.B. Nagy, H. Karge (Eds.), Studies in Surface Science and Catalysis, vol. 125, Elsevier, Amsterdam, 1999, p. 495.
[72] Z. Zsoldos, G. Vass, G. Lu, L. Guczi, Appl. Surf. Sci. 78 (1994) 467.
[73] L. Guczi, J. Mol. Catal. 25 (1984) 13.
[74] J.J. Stephan, V. Ponec, J. Catal. 42 (1976) 1.
[75] R.A. van Santen, in: L. Guczi (Ed.), New Trends in CO Actvation, Elsevier Sci. Publ. Co., Amsterdam, 1991 (Chapter 1).
[76] J.W.A. Sachtler, G.A. Somorjai, Prepr. – Am. Chem. Soc., Div. Pet. Chem. 28 (1983) 491.
[77] P. Biloen, F.M. Dautzenberg, W.M.H. Sachtler, J. Catal. 56 (1977) 77.
[78] J.R.H. van Schaik, R.P. Dessing, V. Ponec, J. Catal. 38 (1975) 273.
[79] S. Galvagno, G. Parravano, J. Catal. 57 (1979) 272.
[80] J.R. Anderson, K. Foger, R.J. Breakspere, J. Catal. 57 (1979) 458.
[81] H.C. de Jongste, V. Ponec, J. Catal. 64 (1980) 228.
[82] M. Haruta, Catal. Today 36 (1997) 153.
[83] M.M. Schubert, S. Hackenberg, A.C. van Veen, M. Muhler, V. Plzak, J. Behm, J. Catal. 197 (2001) 113.
[84] L. Guczi, D. Horváth, Z. Pászti, L. Tóth, Z.E. Horváth, A. Karacs, G. Pető, J. Phys. Chem. B 104 (2000) 3183.
[85] D. Horváth, L. Toth, L. Guczi, Catal. Lett. 67 (2000) 117.
[86] M. Bonarowska, J. Pielaszek, W. Juszczyk, Z. Karpinski, J. Catal. 195 (2000) 304.
[87] A.M. Venezia, V. La Parola, V. Nicoli, G. Deganello, J. Catal. 212 (2002) 56.
[88] D.I. Kochubey, S.N. Pavlova, B.N. Novgorodoc, G.N. Kryukoya, V. Sadykov, J. Catal. 161 (1996) 500.
[89] A. Beck, K. Frey, Z. Koppány, D. Horváth, V. La Parola, L.F. Liotta, G. Pantaleo, A.M. Venezia, L. Guczi, Appl. Catal. A 251 (2003) 359.
[90] L. Guczi, A. Beck, A. Horváth, Zs. Koppány, G. Stefler, I. Sajó, O. Geszti, D. Bazin, J. Lynch, J. Mol. Catal. 204–205 (2003) 545.